Electronic Supplementary Material (ESI) for Nanoscale.
This journal is © The Royal Society of Chemistry 2018

Supplementary Information

Influence of particle size and shape on their margination and wall-adhesion: Implications in Drug Delivery Vehicle design across Nano-to-Micro scale

[1]Michaela Cooley, [2]Apoorva Sarode, [3]Masoud Hoore, [3]Dmitry A. Fedosov, [2]Samir Mitragotri, [1]Anirban Sen Gupta

[1]Case Western Reserve University, Department of Biomedical Engineering, Cleveland, Ohio, USA

[2]Harvard John A Paulson School of Engineering and Applied Sciences, Cambridge, Massachusetts, USA

[3]Theoretical Soft Matter and Biophysics, Institute of Complex Systems and Institute for Advanced Simulation, Forschungszentrum Jülich, Jülich, Germany

Corresponding Author:
Anirban Sen Gupta, PhD
Case Western Reserve University
Department of Biomedical Engineering
10900 Euclid Avenue
Wickenden Building, Rm 517B
Cleveland, Ohio 44106, USA
Phone: 216-368-4564
E-mail: axs262@case.edu

Section S. 1. Computation Models and Simulation Approaches.

Red blood cell and particle membrane model

Membranes are represented by a triangulated mesh of linked vertices and possess elasticity, bending rigidity, and area and volume conservation. To model the elasticity of the membrane, the worm-like chain (WLC) bonds are used between every two linked vertices, as

$$U_{\mathrm{WLC}}(x) = k_{\mathrm{B}}T \frac{l_{\max}}{4\,\xi_{\mathrm{p}}} \frac{3\,x^2 - 2\,x^3}{1 - x}$$

where $l_{\max}$ and ξ_p are respectively the maximum length and persistence length, and $x = l/l_{\max}$ with l being the current bond length. A repulsive potential is added to the WLC potential, in order to have a non-zero equilibrium length for bonds. It is given as

$$U_{\mathrm{POW}}(l) = -\frac{k_p}{1-\alpha}\, l^{1-\alpha}$$

The shear modulus, μ_o can be derived from these potentials.

The bending potential is applied to each pair of adjacent triangles and reads

$$U_b(\theta) = \kappa_b\,(1 - \cos(\theta - \theta_0))$$

where κ_b is the bending constant, which can be related to the bending modulus. θ and θ_0 are respectively the instantaneous and spontaneous angles between the normals of two adjacent triangles sharing the bond.

For area and volume conservation, a harmonic potential is used. For the case of global area, it reads

$$U_A = \frac{1}{2} k_a \frac{(A - A_0)^2}{A_0}$$

where A and A_0 are the instantaneous and spontaneous global areas. Similar harmonic potentials are considered for local triangle areas, and global volume of the whole mesh. The stiffness constants for these potentials are tabulated in Table S. 1.

Table S.1. Membrane properties. $\tau = \eta D_{\mathrm{eff}}^3/\kappa_c$ is the RBC relaxation time, with η, D_{eff}, κ_{c} being the viscosity, the effective diameter of RBCs $D_{\mathrm{eff}} = A/\pi$, and the bending modulus, respectively.

Type	Value	Description
N_{v}	500	Number of vertices
A_0 (μm^2)	133	Global area
V_0 (μm^3)	92.5	Global volume
κ_c/k_BT	70	Bending rigidity
μ_o $\left(D_{\mathrm{eff}}^3/\kappa_c\right)$	4160	Shear modulus
k_a $\left(D_{\mathrm{eff}}^2/\kappa_c\right)$	29600	Global area stiffness
k_d $\left(D_{\mathrm{eff}}^2/\kappa_c\right)$	604	Local area stiffness
k_v $\left(D_{\mathrm{eff}}^3/\kappa_c\right)$	196200	Global volume stiffness

The repulsive part of the Lennard-Jones (LJ) 12-6 potential is applied to the pairwise interaction of RBC vertices between different RBCs, to avoid overlap. The LJ energy is equal to $1k_\mathrm{B}T$, and the LJ length unit is taken equal to the equilibrium bond length between linked vertices.

Fluid model. In 3D, smoothed dissipative particle dynamics (SDPD) is used for fluid particles. In 2D, dissipative particle dynamics (DPD) with higher density is enough to model hydrodynamic effects correctly. In both methods, fluid particles interact through conservative, dissipative, and random forces within a cutoff radius r_c. The SDPD method parameters used in simulations are given in Table S.2. More details on the DPD and SDPD methods are found in References 38,39 and 40 of main manuscript.

Table S.2. SDPD fluid properties. The unit length l and unit mass m are taken as unity and $k_\mathrm{B}T = 0.4$ in the simulations.

Type	Value	Description
$\rho_0 \ (m/l^3)$	3	Reference density
$p_0 \ (k_\mathrm{B}T/l^3)$	250	Reference pressure
$p = p_0 \left(\frac{\rho}{\rho_0}\right)^7 - p_0$		State equation
$\eta \ (\sqrt{mk_\mathrm{B}T}/l^2)$	125	Viscosity
$r_c \ (l)$	1.5	Interaction cutoff

Coupling and boundary conditions

The SDPD fluid particles are coupled to membrane vertices by simple DPD potential without the conservative part. The strength of the coupling is determined by the density of membrane vertices, fluid density, viscosity, etc. The boundary conditions in the flow and vorticity directions are periodic. In the velocity gradient direction, the flow is bound by solid walls, as explained in the main text of the manuscript.

2D simulations

In 2D, the membranes are modeled by closed chains of beads and springs. The bending potential is implemented for each pair of adjacent bonds through an angle potential. The volume conservation is changed to area conservation, while the area conservation is changed to circumference conservation. Instead of SDPD, DPD fluid with a higher density is chosen for modeling hydrodynamic effects. 2D simulation parameters are tabulated in Table S.3.

Table S.3. 2D simulation parameters compared to their 3D counterparts. All other parameters are equal to their 3D counterparts. Here, $D_\mathrm{eff} = L/\pi$, L being the periphery of the 2D cell.

Type	Value	Description
$L \ (l)$	19.2	Periphery
$A \ (l^2)$	13.6	Area
$k_\mathrm{B}T$	1	Thermal energy
$\eta \ (\sqrt{mk_\mathrm{B}T}/l)$	144.4	Viscosity

$\rho_0 \ \ (m/l^2)$	5	Density
$r_c \ \ (l)$	1.5	Interaction cutoff
$a \ \ (k_B T/l)$	40	DPD conservative force constant
$\kappa_c/k_B T$	20	Bending rigidity
$\mu_o \ \ \left(D_{\text{eff}}^2/\kappa_c\right)$	2800	Shear modulus
$k_v \ \ \left(D_{\text{eff}}^2/\kappa_c\right)$	1900	Global area stiffness
$k_a \ \ \left(D_{\text{eff}}/\kappa_c\right)$	306	Global periphery stiffness

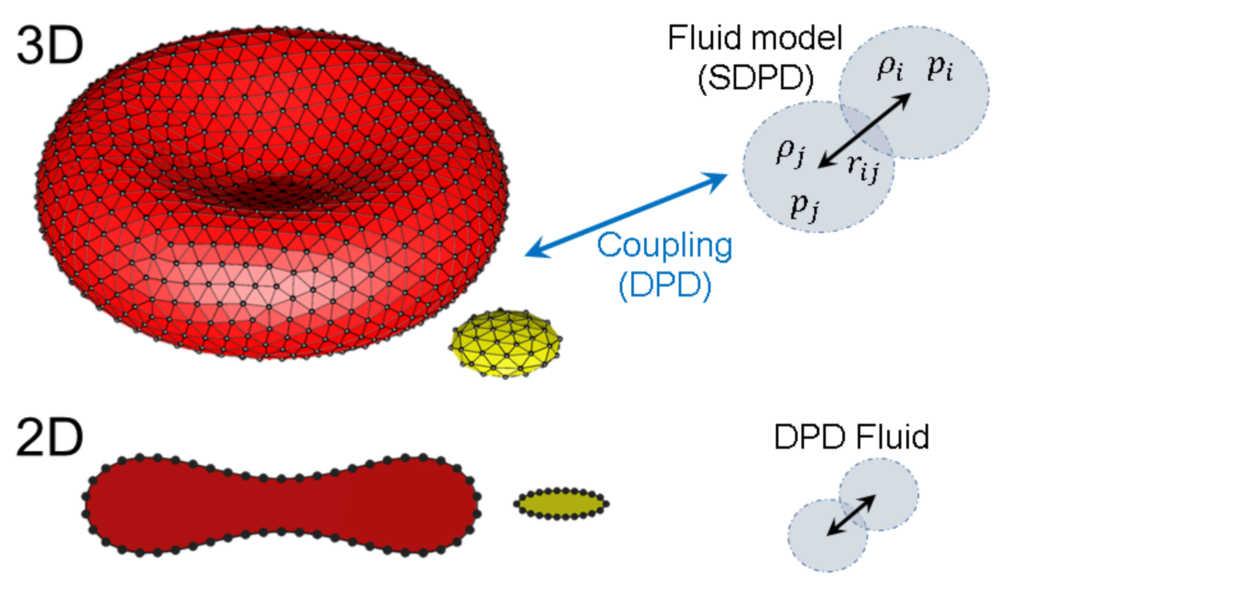

Figure S.1. Schematics of the models used in the 2D and 3D simulations. The membrane vertices are shown with smaller beads than their actual size for more clarity. The 2D membranes have similar dimensions with their 3D counterparts.

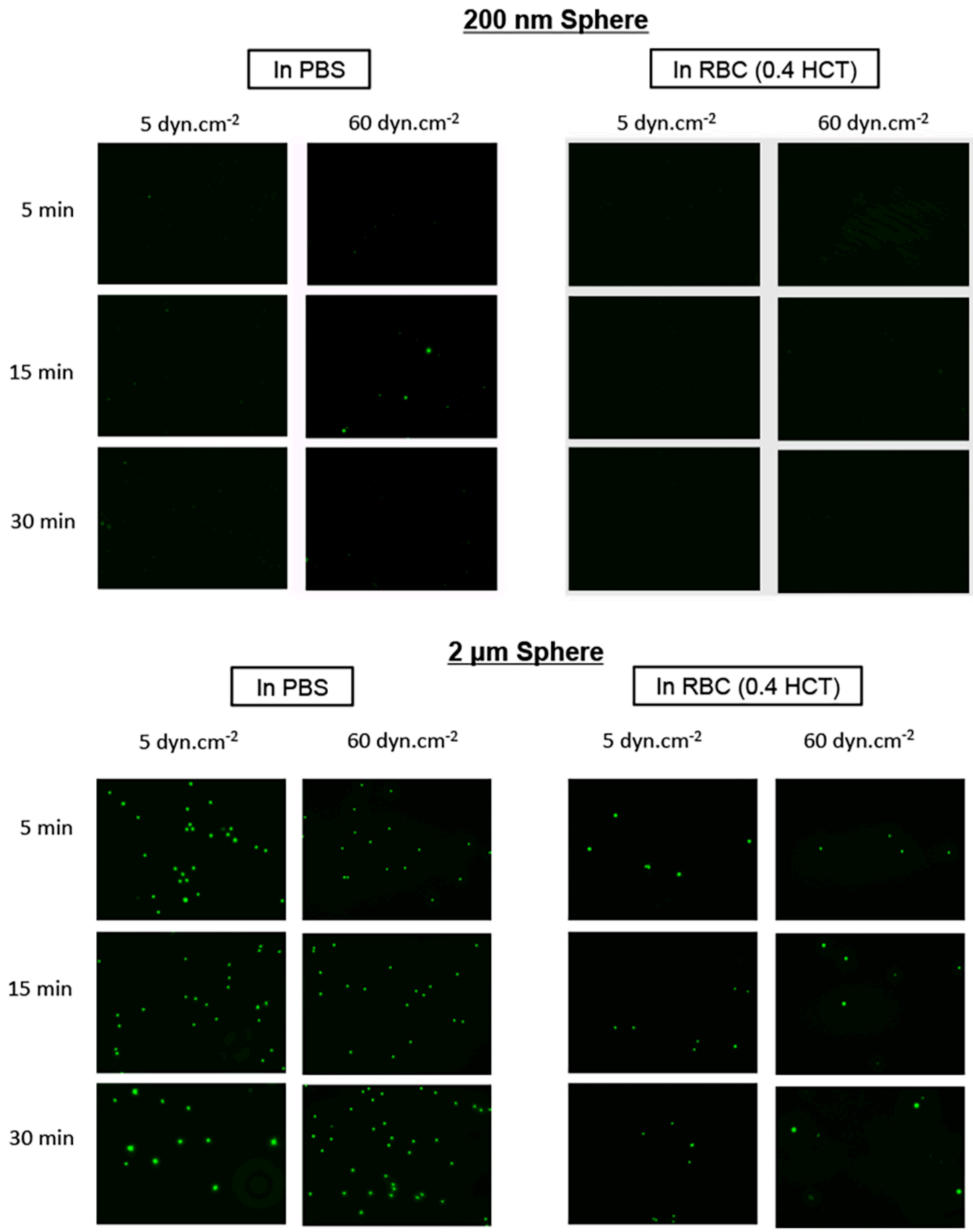

Figure S.2. Representative fluorescent images at 5, 15 and 30 min time-point, comparing adhesion of biotinylated 200 nm diameter PS nanospheres vs. 2 µm diameter PS microspheres adhering to avidin-coated surface under flow of PBS vs. 0.4 HCT (40% v/V RBC) at low (5 dyn.cm^{-2}) and high (60 dyn.cm^{-2}) shear flow conditions.

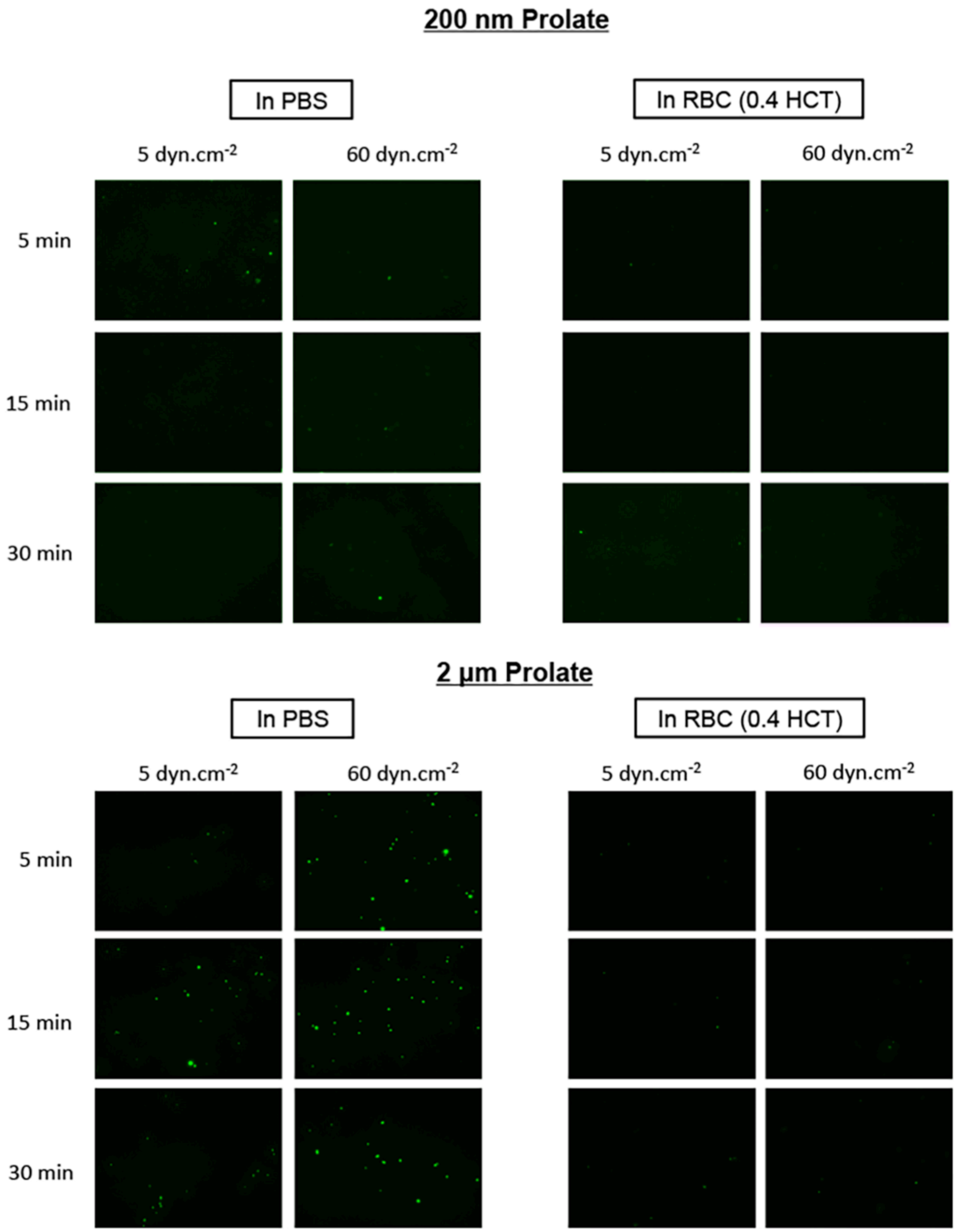

Figure S.3. Representative fluorescent images at 5, 15 and 30 min time-point, comparing biotinylated prolate particles stretched from 200 nm diameter nanospheres vs. 2 µm diameter microspheres, adhering to avidin-coated surface under flow of PBS vs. 0.4 HCT (40% v/V RBC) at low (5 dyn.cm^{-2}) and high (60 dyn.cm^{-2}) shear flow conditions.

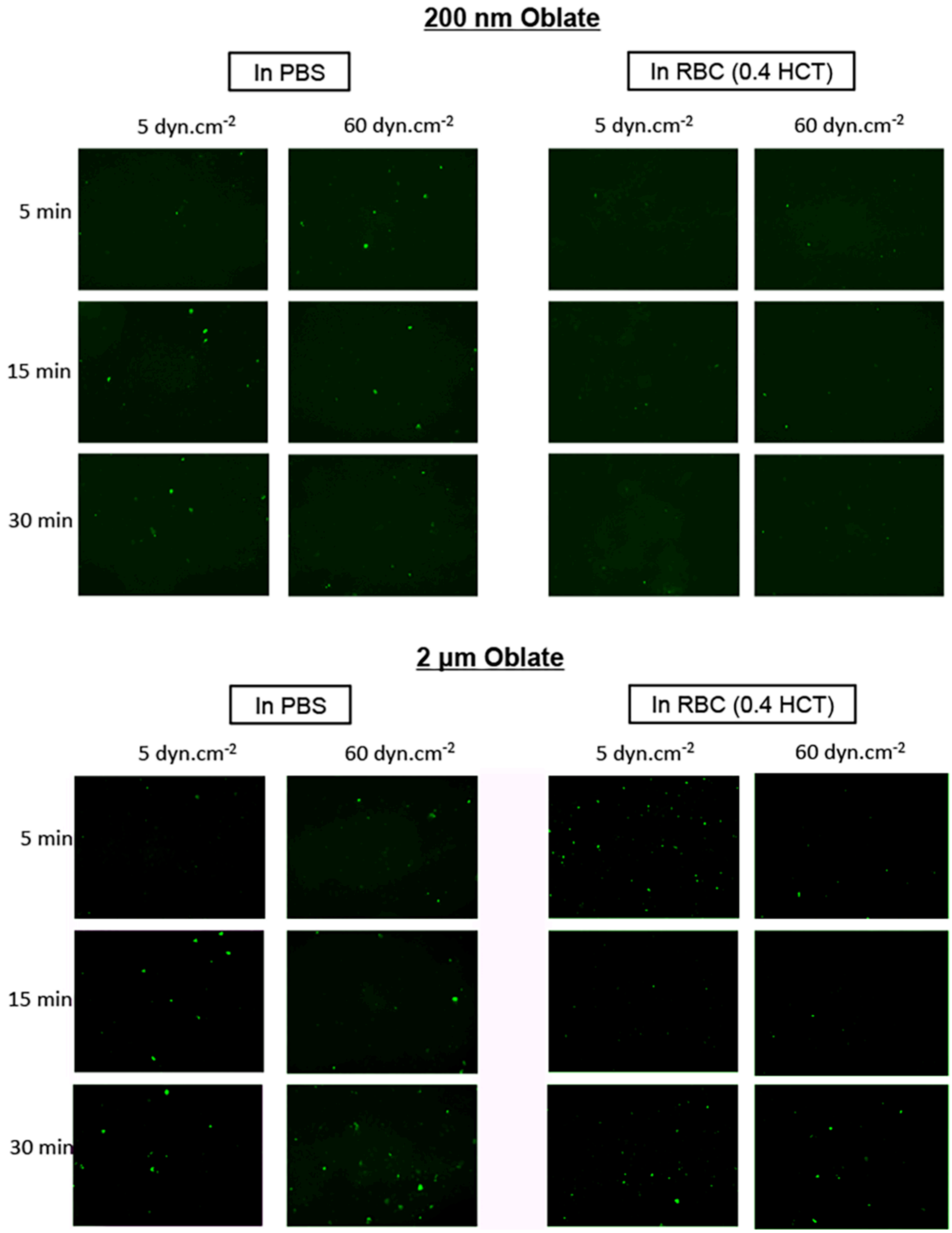

Figure S.4. Representative fluorescent images at 5, 15 and 30 min time-point, comparing biotinylated oblate (discoid) particles stretched from 200 nm diameter PS nanospheres vs. 2 µm diameter PS microspheres, adhering to avidin-coated surface under flow of PBS vs. 0.4 HCT (40% v/V RBC) at low (5 dyn.cm^{-2}) and high (60 dyn.cm^{-2}) shear flow conditions.

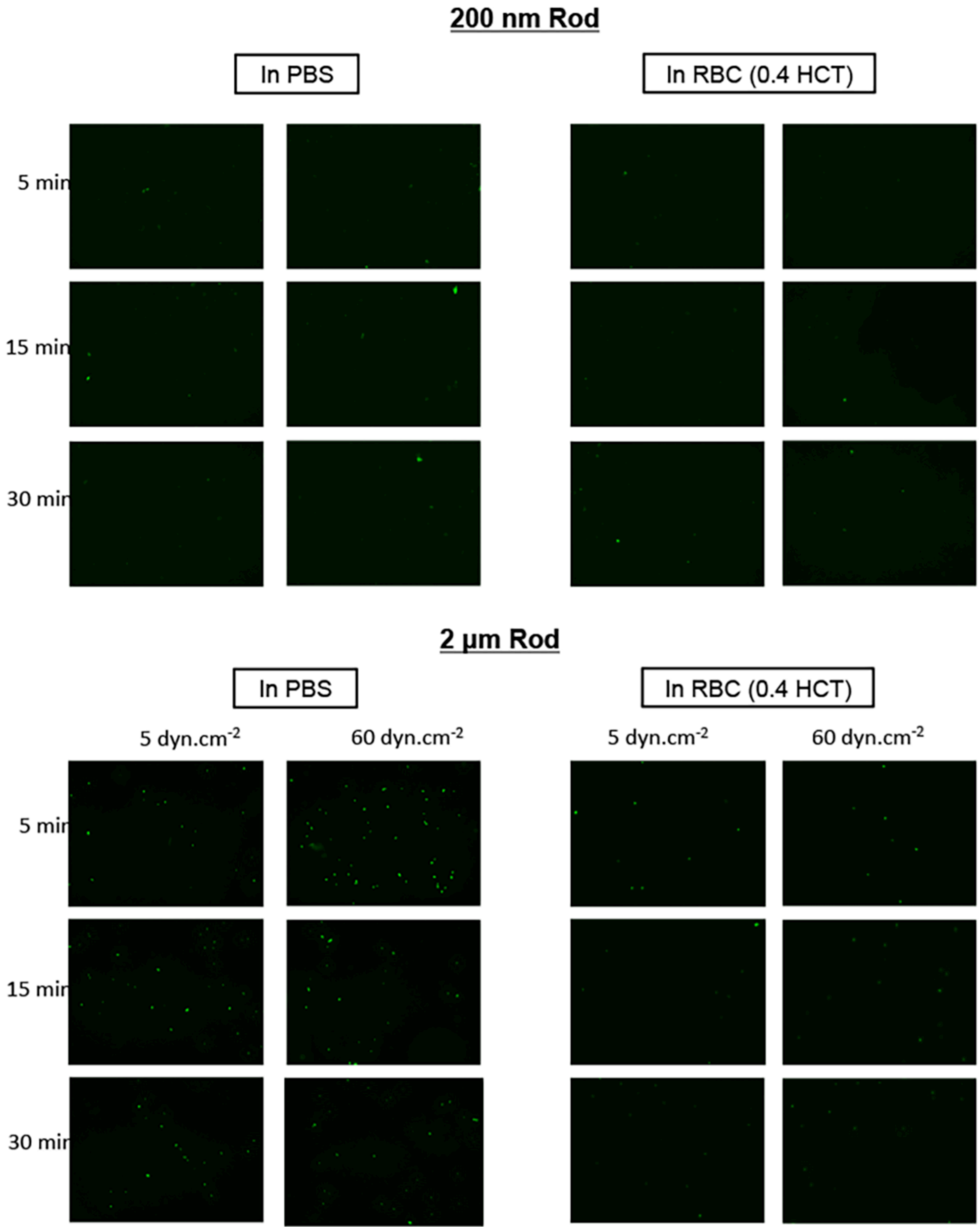

Figure S.5. Representative fluorescent images at 5, 15 and 30 min time-point, comparing biotinylated rod-shaped particles stretched from 200 nm diameter PS nanospheres vs. 2 μm diameter PS microspheres, adhering to avidin-coated surface under flow of PBS vs. 0.4 HCT (40% v/V RBC) at low (5 dyn.cm^{-2}) and high (60 dyn.cm^{-2}) shear flow conditions.

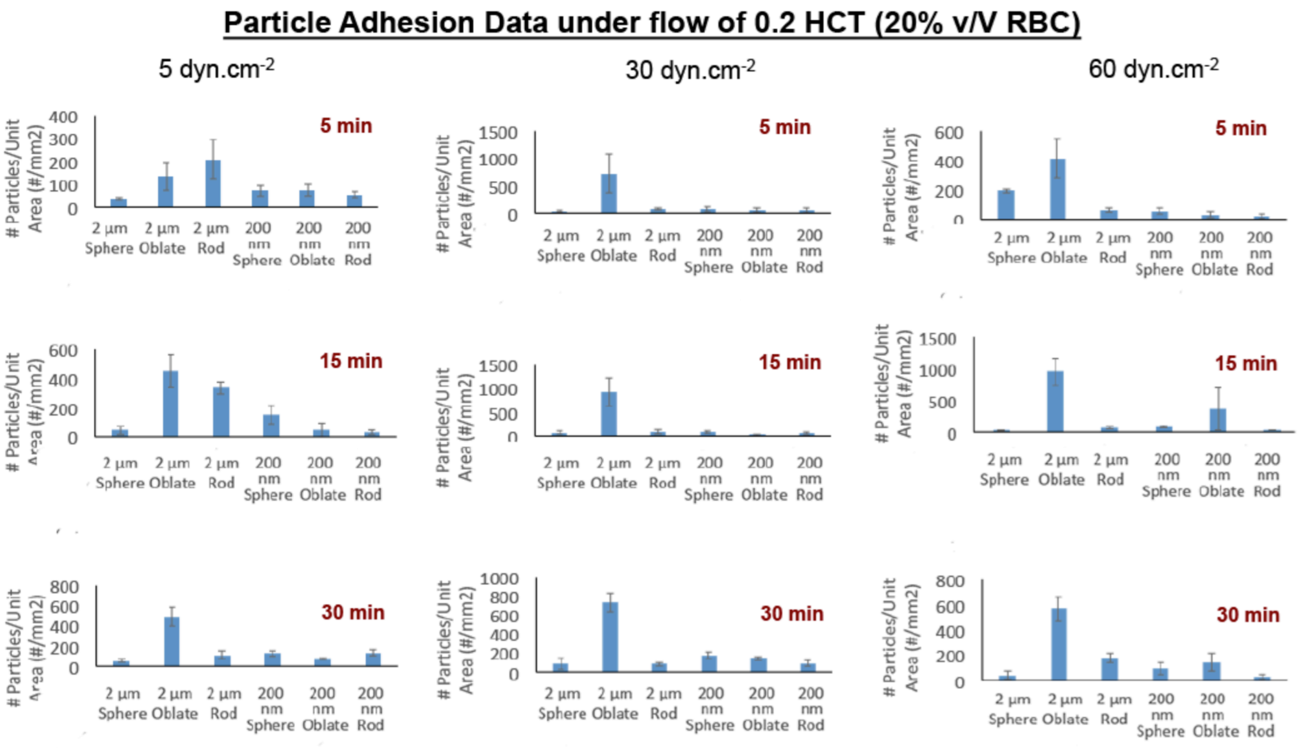

Figure S.6. Adhesion data of biotinylated particles of various shapes and sizes binding to avidin-coated surface in parallel plate flow chamber under flow of 0.2 HCT (20% v/V RBCs) at low (5 dyn.cm-2), moderate (30 dyn.cm-2) and high (60 dyn.cm-2) conditions; Results indicate that in presence of 0.2 HCT flow, over time, non-spherical particles show higher adhesion and retention at the wall compared to spherical particles, and microscale ellipsoid (oblate) particles show the highest levels of wall-adhesion; This trend was found to be also conserved at physiological RBC (0.4 HCT) flow as indicated in Figures 6 and 7 of main manuscript.

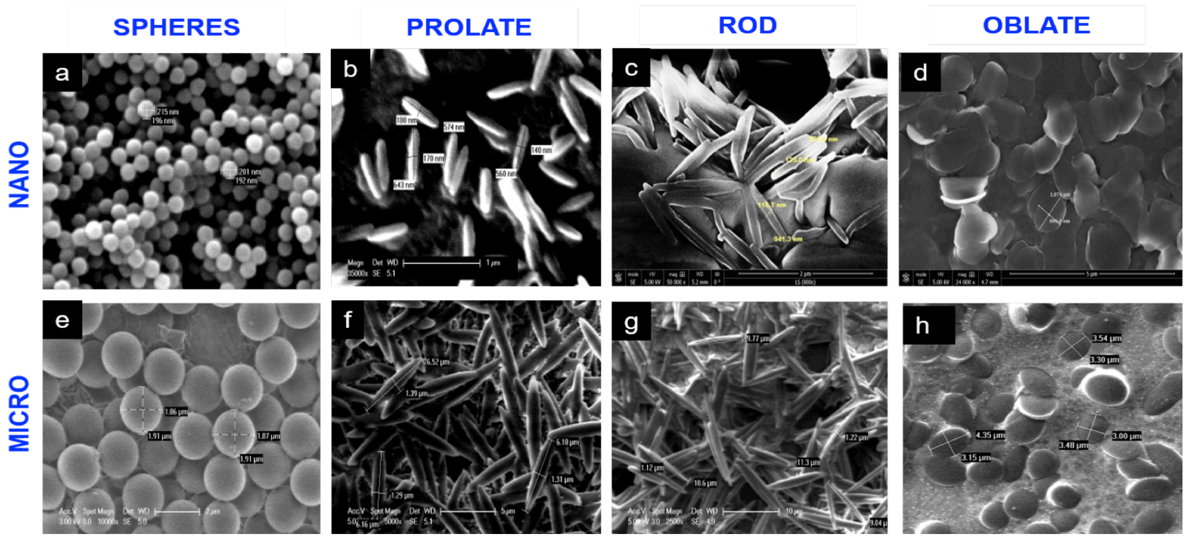

Figure S.7. Scanning electron micrographs of biotinylated particles with spherical, prolate (AR5), rod (AR10) and oblate (discoid) geometries; the biotinylation method is described in the Methods section of the main manuscript. As evident, the biotinylation process did not impact the overall starting geometry of the particles.

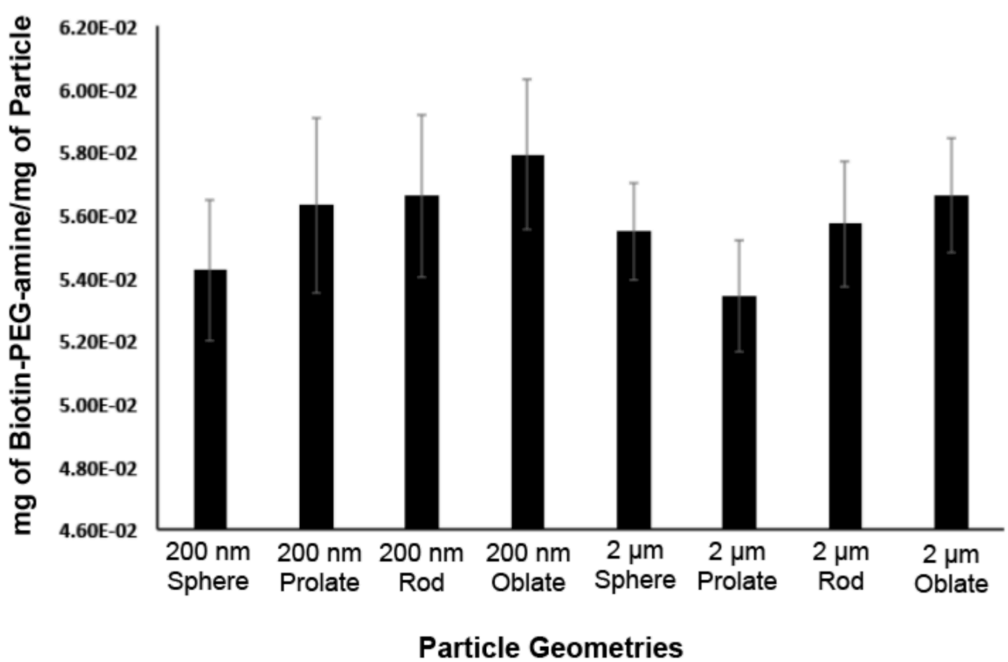

Figure S.8. HABA assay based characterization of surface-biotinylation on nanoparticles and microparticles of various geometries representative of the library of particles studied for adhesion capabilities on avidin-coated slides in microfluidic chamber.